

Quadratic fractional solitons

Liangwei Zeng,¹ Yongle Zhu,¹ Boris A. Malomed,^{2,3} Dumitru Mihalache,⁴
Qing Wang,⁵ Hu Long,¹ Yi Cai,¹ Xiaowei Lu,¹ and Jingzhen Li^{1,*}

¹*Shenzhen Key Laboratory of Micro-Nano Photonic Information Technology,
Key Laboratory of Optoelectronic Devices and Systems of Ministry of Education and Guangdong Province,
College of Physics and Optoelectronic Engineering, Shenzhen University, Shenzhen 518060, China*

²*Department of Physical Electronics, School of Electrical Engineering, Faculty of Engineering,
and Center for Light-Matter Interaction, Tel Aviv University, P.O.B. 39040, Tel Aviv, Israel*

³*Instituto de Alta Investigación, Universidad de Tarapacá, Casilla 7D, Arica, Chile*

⁴*Horia Hulubei National Institute of Physics and Nuclear Engineering, Magurele, Bucharest, RO-077125, Romania*

⁵*College of Science, JiuJiang University, Jiujiang 334000, Jiangxi, China*

We introduce a system combining the quadratic self-attractive or composite quadratic-cubic nonlinearity, acting in the combination with the fractional diffraction, which is characterized by its Lévy index α . The model applies to a gas of quantum particles moving by Lévy flights, with the quadratic term representing the Lee-Huang-Yang correction to the mean-field interactions. A family of fundamental solitons is constructed in a numerical form, while the dependence of its norm on the chemical potential characteristic is obtained in an exact analytical form. The family of *quasi-Townes solitons*, appearing in the limit case of $\alpha = 1/2$, is investigated by means of a variational approximation. A nonlinear lattice, represented by spatially periodical modulation of the quadratic term, is briefly addressed too. The consideration of the interplay of competing quadratic (attractive) and cubic (repulsive) terms with a lattice potential reveals families of single-, double-, and triple-peak gap solitons (GSs) in two finite bandgaps. The competing nonlinearity gives rise to alternating regions of stability and instability of the GS, the stability intervals shrinking with the increase of the number of peaks in the GS.

Keywords: Fractional diffraction; Lévy index; Lee-Huang-Yang corrections; Competing nonlinearities; Townes solitons; Gap solitons.

I. INTRODUCTION

It is commonly known that soliton families are supported by the nonlinear Schrödinger equation (NLSE) [1–12] [alias the Gross-Pitaevskii equation (GPE) for Bose-Einstein condensates (BECs) [13, 14]] in a great number of realizations. Still broader varieties of solitons have been predicted in generalized models of the NLSE type, such as ones with the strength of the repulsive nonlinearity rapidly growing from the center to periphery [15–23]. Solitons in linear [24–34] and nonlinear spatially periodic potentials [35–37] (alias linear/nonlinear lattices) have also been a subject of many works. Recently, defects in linear [34] and nonlinear [38] lattices have been demonstrated to stabilize different types of solitons. Linear periodic potentials form spectral bandgaps [39], which are populated by gap-soliton (GS) families, which include fundamental, multipole, and vortex modes. GSs have been widely studied theoretically [29, 31, 39] and observed in experiments [40–42].

The introduction of fractional calculus in NLSE has been drawing much interest since it was proposed by Laskin (originally, in the linear form) as the quantum-mechanical model, derived from the respective Feynman-integral formulation, for particles moving by Lévy flights [43–45]. Experimental implementation of fractional linear Schrödinger equations has been reported in condensed matter [46, 47], optics [48] (in the form of transverse dynamics in laser cavities), and quan-

tum physics [49]. Further, realization of the propagation dynamics of light beams governed by this equation was proposed [50], and its extension for the model including the \mathcal{PT} symmetry was put forward too [51]. Many types of optical solitons produced by fractional NLSEs have been theoretically investigated [52]–[79], such as “accessible solitons” [54, 55], GSs [59–63], solitary vortices [64, 65], multipole and multi-peak solitons [66–69], soliton clusters [70], symmetry-breaking solitons [73–75] as well as solitons in couplers [77–79].

Still missing is the analysis of settings combining the fractional diffraction/dispersion and quadratic nonlinearity, except for a brief mention of the possibility to derive a two-component system of equations for the second-harmonic generation in the fractional-dimension space [80]. In this work, we introduce a model combining the self-attractive quadratic nonlinearity, or competing attractive-repulsive quadratic-cubic (QC) nonlinearity, and the fractional diffraction. A linear lattice potential is also included, in the general case. The model is an amended GPE for the description of a quasi-one-dimensional BEC composed of particles moving by Lévy flights, with the cubic nonlinearity representing, as usual, contact interactions between particles, treated in the mean-field approximation [13]. The sign of the cubic term may correspond to either repulsive or attractive inter-particle interactions. The quadratic term represents the beyond-mean-field correction induced by quantum fluctuations around mean-field states [the Lee-Huang-Yang (LHY) effect [81]], in a binary BEC with contact repulsion between identical particles and attraction between ones representing different species in the

* lijz@szu.edu.cn

two-component mixture. In the three-dimensional (3D) form, the LHY correction, in the form of a quartic self-repulsive term (assuming equal wave functions of the two components), was derived by Petrov [82] (see also Ref. [83]). The accordingly amended GPE had predicted the existence of stable 3D and quasi-2D self-trapped states in the form of “quantum droplets” (QDs), which were quickly demonstrated experimentally [84–87]. The reduction of the dimension from 3 to 1 leads to the replacement of the repulsive quartic LHY term by an *attractive* quadratic one [88], which leads to the prediction of specific quasi-1D QDs [89] and intrinsic modes in them [90]. This quadratic term plays the central role in the analysis presented in this work.

First, we address the basic version of the model, with the quadratic-only nonlinearity acting in the free space (without the lattice potential), construct a family of fundamental solitons in it, and identify their stability region. The consideration of the setting without the cubic term is relevant because it may be eliminated by means of the Feshbach resonance, adjusting the strength of the inter-species interaction in the binary BEC [91]. The resulting *LHY fluid* has been observed experimentally [92]. Then, we demonstrate that the interplay of the general QC nonlinearity, which includes competing self-attractive quadratic and repulsive cubic terms, with the underlying lattice potential creates various types of gap solitons, including two- and three-peak ones. The system with the competing nonlinearities is interesting, as the previous study of gap solitons in the fractional setting has produced very different results for the self-repulsive and attractive signs of the cubic term [59], while competing nonlinearities were not considered there.

The rest of this paper is organized as follows. We formulate the model, including scaling relations and the variational approximation (VA) for soliton families in the free-space setting in Sec. II. Numerical results for the basic case of the self-attractive quadratic LHY nonlinearity in the free space are reported in Sec. III, which also presents, for the sake of comparison, similar results based on the cubic self-attraction. In addition, the same Section briefly addresses solitons supported by the quadratic nonlinear lattice, with the self-attraction coefficient subject to spatially periodic modulation. Results for families of single-, double-, and triple-peak GSs, supported by the competing QC nonlinearity, combined with the lattice potential, are summarized in Sec. IV. Finally, the paper is concluded by Sec. V.

II. THE MODEL AND VARIATIONAL APPROXIMATION

A. Basic equations

In the scaled form, the LHY-amended fractional GPE, for identical wave functions Ψ of the two components of the binary BEC composed of particles moving by Lévy flights, is

written as

$$i\frac{\partial\Psi}{\partial t} = \frac{1}{2}\left(-\frac{\partial^2}{\partial x^2}\right)^{\alpha/2}\Psi + V(x)\Psi + \xi|\Psi|\Psi + g|\Psi|^2\Psi. \quad (1)$$

Here t and x are the normalized time and coordinate, while $\xi < 0$ and $g > 0/g < 0$ are the coefficients of the attractive quadratic (LHY) and repulsive/attractive cubic (mean-field) nonlinearities, respectively. The fractional-diffraction operator with Lévy index (LI) α is defined, as usual, by means of the Fourier transform (also called the Riesz derivative): [43–49, 53]:

$$\left(-\frac{\partial^2}{\partial x^2}\right)^{\alpha/2}\Psi = \frac{1}{2\pi}\int_{-\infty}^{+\infty} ds|s|^\alpha \int_{-\infty}^{+\infty} d\eta e^{is(x-\eta)}\Psi(\eta), \quad (2)$$

the normal diffraction corresponding to $\alpha = 2$. The lattice potential in Eq. (1) with strength V_0 is taken as

$$V = V_0 \sin^2 x \quad (3)$$

(in the free space, $V_0 = 0$).

We look for stationary solutions to Eq. (1) with a real chemical potential μ in the form of

$$\Psi = U(x)\exp(-i\mu z). \quad (4)$$

The substitution of Ψ in Eq. (1), leads to the stationary equation,

$$\mu U = \frac{1}{2}\left(-\frac{\partial^2}{\partial x^2}\right)^{\alpha/2}U + V(x)U + \xi|U|U + g|U|^2U. \quad (5)$$

The stationary localized states are characterized by their norm,

$$N = \int_{-\infty}^{+\infty} |U(x)|^2 dx. \quad (6)$$

To introduce the linear-stability analysis for the stationary states, the perturbed solution is defined as

$$\Psi = [U(x) + p(x)\exp(\lambda t) + q^*(x)\exp(\lambda^* t)]\exp(-i\mu t), \quad (7)$$

where $p(x)$ and $q^*(x)$ are small complex perturbations (the asterisk denotes complex conjugation), and λ is the instability growth rate. Substituting this ansatz in Eq. (1), one derives the linearized Bogoliubov-de Gennes equations for p and q :

$$\begin{cases} i\lambda p = +\frac{1}{2}\left(-\frac{\partial^2}{\partial x^2}\right)^{\alpha/2}p + (V - \mu)p + gU^2(2p + q) \\ \quad + \frac{1}{2}\xi|U|(3p + q), \\ i\lambda q = -\frac{1}{2}\left(-\frac{\partial^2}{\partial x^2}\right)^{\alpha/2}q + (\mu - V)q - gU^2(2q + p) \\ \quad - \frac{1}{2}\xi|U|(3q + p). \end{cases} \quad (8)$$

This form of the equations is valid only in the case when the underlying stationary solution $U(x)$ is a real one [the presence of $|U|$ in Eq. (8) is relevant if $U(x)$ is a sign-changing function]. The underlying stationary solution (4) is stable solely in the case when Eq. (8) produces purely imaginary eigenvalues λ .

B. Scaling relations for soliton families

In the case of the attractive cubic-only nonlinearity in the free space, with

$$\xi = V = 0, g < 0, \quad (9)$$

Eq. (5) gives rise to the exact scaling relation between the soliton's norm and chemical potential:

$$N_{\text{cubic}}(\mu; g) = N_{\text{cubic}}^{(0)}(\alpha) |g|^{-1} (-\mu)^{1-1/\alpha}, \quad (10)$$

with a constant $N_{\text{cubic}}^{(0)}(\alpha)$ [for the usual NLSE, it is $N_{\text{cubic}}^{(0)}(\alpha = 2) = 2\sqrt{2}$, see Eq. (26) below]. The fact that this relation satisfies the commonly known Vakhitov-Kolokolov (VK) criterion, $dN/d\mu < 0$ [93, 94], at $\alpha > 1$, suggests that the respective soliton family may be stable, see further details in Figs. 3 and 4 below. The case of $\alpha = 1$, which corresponds to the degenerate form of relation (10), with $N_{\text{cubic}}(\mu) \equiv \text{const}$, implies the occurrence of the *critical collapse*, which makes all solitons unstable (cf. the commonly known cubic NLSE in the 2D space with the normal diffraction, $\alpha = 2$, in which the family of *Townes' solitons*, destabilized by the critical collapse, have a constant norm [94]). In the case of $\alpha < 1$, the solitons generated by Eq. (5) with $\xi = V = 0$ and $g < 0$ are strongly destabilized by the presence of the *supercritical collapse*, similar to the solitons of the usual cubic NLSE in three dimensions [94].

In the case of the quadratic self-attraction in the free space,

$$g = V = 0, \xi < 0, \quad (11)$$

a scaling relation for the soliton's norm, similar to Eq. (10), is

$$N_{\text{quadr}}(\mu; \xi) = N_{\text{quadr}}^{(0)}(\alpha) |\xi|^{-2} (-\mu)^{2-1/\alpha}, \quad (12)$$

with a constant $N_{\text{quadr}}^{(0)}(\mu)$ [in the case of the usual diffraction, $N_{\text{quadr}}^{(0)}(\alpha = 2) = 3\sqrt{2}$, see Eq. (25) below]. Equation (12) demonstrates that the respective solitons satisfy the VK stability criterion at $\alpha > 1/2$. Equation (5) with the quadratic nonlinearity gives rise to the degenerate family of *quasi-Townes* solitons with a constant norm, which are destabilized by the presence of the critical collapse, at $\alpha = 1/2$. The subcritical collapse takes place at $\alpha < 1/2$.

In the QC model including both $g < 0$ and $\xi < 0$ in Eq. (5), the scaling relations (10) and (12) dominate, respectively, at $|\mu| \rightarrow \infty$ and $|\mu| \rightarrow 0$. In the latter limit, the relation (12) is relevant too for the QC model with the competing quadratic self-attraction and cubic repulsion, i.e., $\xi < 0$ and $g > 0$. In the system with the competing nonlinearities, the solitons exist in the interval of the chemical potential that was identified for QDs in Ref. [89]:

$$\mu_{\text{min}} \equiv -2\xi^2 / (9g) < \mu < 0. \quad (13)$$

In the limit of $\mu \rightarrow \mu_{\text{min}}$, the solitons develop the shape of flat-top QDs (see Ref. [89]), with the local density approaching the limit value,

$$U_{\text{max}}^2 = (2\xi/3g)^2, \quad (14)$$

and a logarithmically large length,

$$l \simeq (-2\mu)^{1/\alpha} \ln \left((\mu - \mu_{\text{min}})^{-1} \right). \quad (15)$$

Such flat-top solitons are stable, and they support a large number of oscillatory internal modes [90].

C. The variational approximation (VA)

In the context of a different problem, it was recently demonstrated that VA can be used to look for localized solutions of the fractal NLSE [72, 95]. To this end, we note that Eq. (5) for real $U(x)$, with the fractional diffraction operator defined as per Eq. (2) can be derived from the Lagrangian (see also Ref. [96]),

$$\begin{aligned} L = & \frac{1}{8\pi} \int_{-\infty}^{+\infty} ds |s|^\alpha \int_{-\infty}^{+\infty} d\eta \int_{-\infty}^{+\infty} dx e^{is(x-\eta)} U(x) U(\eta) \\ & + \frac{1}{2} \int_{-\infty}^{+\infty} dx [-\mu + V(x)] U^2(x) \\ & + \frac{\xi}{3} \int_{-\infty}^{+\infty} dx U^3(x) + \frac{g}{4} \int_{-\infty}^{+\infty} dx U^4(x). \end{aligned} \quad (16)$$

A natural form of the ansatz approximating the solitons sought for is based on the Gaussian,

$$U(x) = A \exp \left(-\frac{x^2}{2W^2} \right), \quad (17)$$

with real amplitude A , width W , and the norm calculated as per Eq. (6),

$$\mathcal{N} = \sqrt{\pi} A^2 W \quad (18)$$

(the calligraphic font is used to denote quantities pertaining to the VA). The substitution of the ansatz in Lagrangian (16) yields the corresponding effective Lagrangian, which is written here with the amplitude A replaced by the norm, pursuant to Eq. (18), and the lattice potential taken as per Eq. (3):

$$\begin{aligned} L_{\text{eff}} = & \frac{1}{2} \left(\frac{V_0}{2} - \mu \right) \mathcal{N} - \frac{V_0}{4} \mathcal{N} e^{-W^2} + \frac{\Gamma((1+\alpha)/2)}{4\sqrt{\pi}} \frac{\mathcal{N}}{W^\alpha} \\ & + \frac{\sqrt{2}\xi}{3\sqrt{3}\pi^{1/4}} \frac{\mathcal{N}^{3/2}}{\sqrt{W}} + \frac{g}{4\sqrt{2}\pi} \frac{\mathcal{N}^2}{W}, \end{aligned} \quad (19)$$

where Γ is the Gamma-function. Then, values of \mathcal{N} and W are predicted by the Euler-Lagrange equations,

$$\partial L_{\text{eff}} / \partial \mathcal{N} = \partial L_{\text{eff}} / \partial W = 0. \quad (20)$$

The most essential result of the VA is the prediction of the fixed value of the norm for the *quasi-Townes* solitons, for which the critical collapse takes place in the free space ($V_0 = 0$) at $\alpha = 1/2$ and $\alpha = 1$ in the cases defined, respectively, by Eqs. (11) and (9), i.e., with the quadratic-only or cubic-only nonlinearity:

$$\left(\mathcal{N}_{\text{Townes}}^{(\text{quadr})} \right)_{\text{VA}} = \frac{27}{32\sqrt{\pi}} \Gamma^2 \left(\frac{3}{4} \right) \approx 0.71, \quad (21)$$

$$\left(\mathcal{N}_{\text{Townes}}^{(\text{cubic})} \right)_{\text{VA}} = \sqrt{2} \approx 1.41 \quad (22)$$

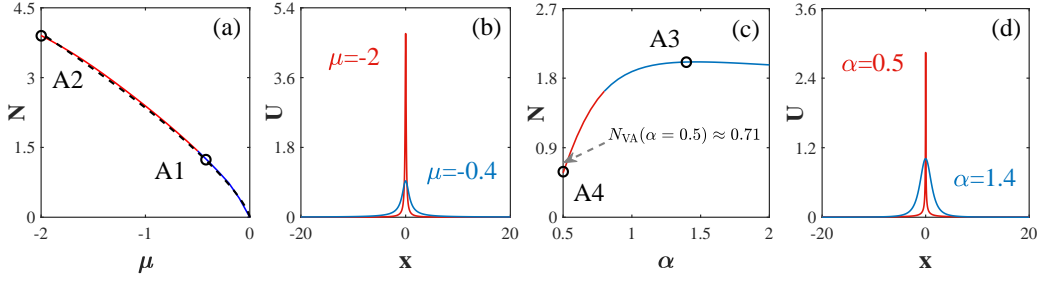


FIG. 1. (a) The dependence $N(\mu)$ and (b) the profiles of solitons labeled A1 and A2 in (a) (corresponding to $\mu = -0.4$ and -2 , respectively) for the soliton family produced by the numerical solution of Eq. (5) with the quadratic-only nonlinearity ($\xi = -1$, $g = 0$) in the free space ($V = 0$), at a fixed LI, $\alpha = 0.8$. (c) The dependence $N(\alpha)$ and (d) the profiles of solitons labeled A3 and A4 (corresponding to $\alpha = 1.4$ and 0.5 , respectively) for a fixed chemical potential, $\mu = -0.6$. The blue and red segments of the curves in panels (a) and (c) denote subfamilies of stable and (weakly) unstable solitons, respectively. The black dashed line in (a) represents the analytical scaling relation (12). The value marked by the gray dashed arrow is the one predicted by Eq. (21), its numerically found counterpart being $N_{\text{numer}}(\alpha = 0.5) \approx 0.57$. The evolution of the solitons labeled by A1–A4 are displayed in Fig. 2.

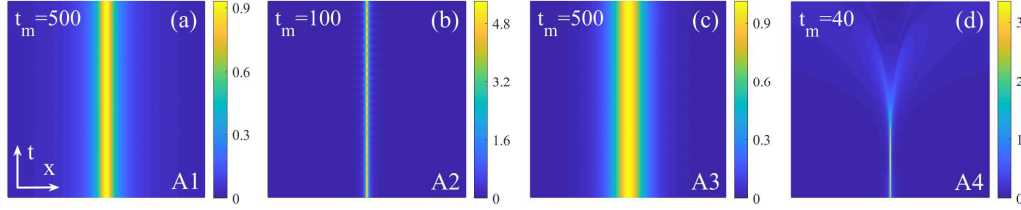


FIG. 2. The perturbed evolution of the solitons corresponding to labels A1–A4 in Figs. 1(a,c). The respective values of the parameters are $\alpha = 0.8$, $\mu = -0.4$ (a); $\alpha = 0.8$, $\mu = -2$ (b); $\alpha = 1.4$, $\mu = -0.6$ (c); $\alpha = 0.5$, $\mu = -0.6$ (d). Other parameters are $\xi = -1$, $g = V_0 = 0$. In all panels, the evolution is plotted in the interval $-10 < x < +10$, while the values t_m indicate time intervals in the respective panels, $0 < t < t_m$. The value of t_m is taken large in panels (a) and (c), to verify the complete stability of the respective solitons.

[Eq. (22) is tantamount to a result recently reported for the cubic nonlinearity with $\alpha = 1$ in Ref. [72]]. These results may be likened to the well-known VA prediction for the norm of the Townes' solitons in the 2D NLSE with the cubic self-focusing [97]: $(N_{\text{Townes}}^{(2D-\text{cubic})})_{\text{VA}} = 2\pi$, while the respective numerical value is $N_{\text{Townes}}^{(2D-\text{cubic})} \approx 5.85$, the relative error of the VA being $\approx 7\%$. It is shown below in Figs. 1(c) and 3(c) that numerically found counterparts of values (21) and (22) are

$$(N_{\text{Townes}}^{(\text{quadr})})_{\text{num}} \approx 0.57, \quad (23)$$

$$(N_{\text{Townes}}^{(\text{cubic})})_{\text{num}} \approx 1.23. \quad (24)$$

As well as in the above-mentioned case, the VA predicts the Townes' norms that are somewhat larger than their numerically found counterparts, with the error $\approx 20\%$ and 13% for the quadratic and cubic nonlinearities, respectively. A relatively large size of the error is a consequence of the complex structure of the nonlinear equation with the fractional diffraction.

The VA also predicts if the dependence $N(\alpha)$ for a fixed value of μ is growing or decaying. To this end, we note that, at $\alpha = 2$, the usual NLSE with the quadratic or cubic non-

linearity gives rise to the following $N(\mu)$ dependences for the commonly known soliton solutions:

$$N_{\alpha=2}^{(\text{quadr})} = 3\sqrt{2}(-\mu)^{3/2}, \quad (25)$$

$$N_{\alpha=2}^{(\text{cubic})} = 2\sqrt{-2\mu}. \quad (26)$$

Comparing these with values (21) and (22), one arrives at the conclusion that, in the case of the quadratic-only nonlinearity, the $N(\alpha)$ dependence is growing at $-\mu > -\mu_{\text{crit}}^{(\text{quadr})} \approx 0.305$, and is decaying at $-\mu < -\mu_{\text{crit}}$. Similarly, $-\mu_{\text{crit}}^{(\text{cubic})} = 1/4$ for the cubic-only term. These predictions agree with the numerical results displayed below in Figs. 1(c) and 3(c), respectively.

Finally, it is relevant to mention that the inclusion of the external potential, such as the periodic one given by Eq. (3), helps to suppress the collapse in the fractional NLSE, and thus to extend the range of the existence of solitons [67]. In the present case, this possibility can be illustrated by results following from Eqs. (19) and (20), which include the weak potential with small $V_0 > 0$, for the model with the quadratic nonlinearity ($\xi = -1$, $g = 0$). Namely, at $\alpha = 1/2$ the degeneracy of the soliton's norm is (slightly) lifted by the lattice

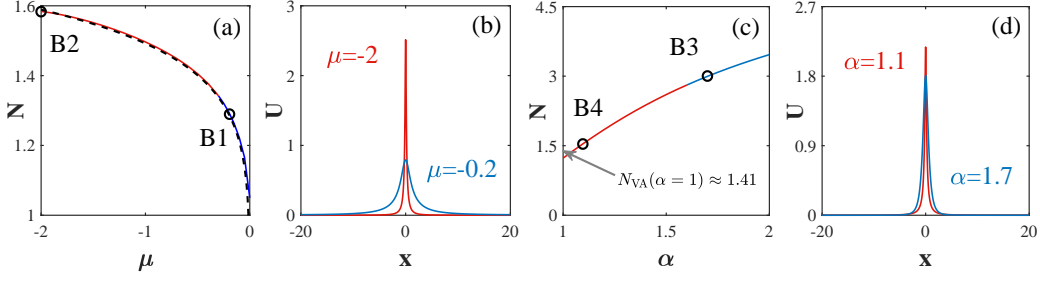


FIG. 3. (a) The dependence $N(\mu)$ and (b) the profiles of solitons labeled B1 and B2 in (a) (corresponding to $\mu = -0.2$ and -2 , respectively) for the soliton family produced by the numerical solution of Eq. (5) with the cubic-only nonlinearity ($\xi = 0, g = -1$) in the free space ($V = 0$), at a fixed LI, $\alpha = 1.1$. (c) The dependence $N(\alpha)$ and (d) the profiles of solitons labeled B3 and B4 (corresponding to $\alpha = 1.7$ and 1.1 , respectively) for a fixed chemical potential, $\mu = -1.5$. The blue and red segments of the curves in panels (a) and (c) denote subfamilies of stable and (weakly) unstable solitons, respectively. The black dashed line in (a) represents the analytical scaling relation (10). The value marked by the gray dashed arrow is predicted by the VA, as per Eq. (22). Its numerically found counterpart is $N_{\text{numer}}(\alpha = 1) \approx 1.41$. The evolution of the solitons labeled by B1–B4 is displayed in Fig. 4.

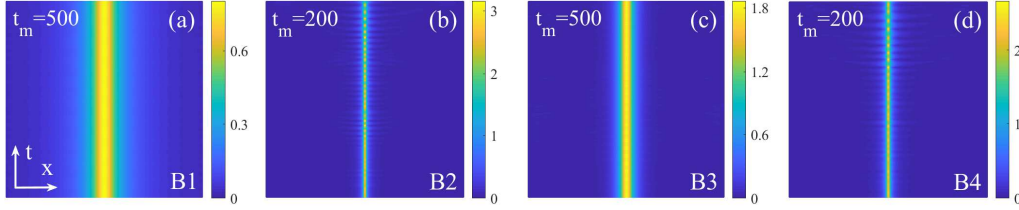


FIG. 4. The perturbed evolution of the solitons corresponding to labels B1–B4 in Figs. 3(a,c). The respective values of the parameters are $\alpha = 1.1, \mu = -0.2$ (a); $\alpha = 1.1, \mu = -2$ (b); $\alpha = 1.7, \mu = -1.5$ (c); and $\alpha = 1.1, \mu = -1.5$ (d). Other parameters are $g = -1, \xi = V_0 = 0$. In all panels, the evolution is plotted in interval $-10 < x < +10$. The values t_m indicate time intervals in the respective panels, $0 < t < t_m$.

potential, allowing the solitons to attain the smallest norm

$$\begin{aligned} & \left(\mathcal{N}_{\min}^{(\text{quadr})}(\alpha = 1/2) \right)_{\text{VA}} \\ & \approx \left(\mathcal{N}_{\text{Townes}}^{(\text{quadr})} \right)_{\text{VA}} - \frac{27(5/e)^{5/4}}{16\sqrt{2}} \Gamma\left(\frac{3}{4}\right) V_0 \quad (27) \\ & \approx 0.71 - 3.13V_0, \end{aligned}$$

cf. Eq. (21). Further, the value of α at which the critical collapse takes place (i.e., the value above which solitons exist) is lowered by the weak lattice potential from $1/2$ to

$$\begin{aligned} \alpha_{\text{crit}}^{(\text{quadr})} & \approx \frac{1}{2} - \frac{2\sqrt{2\pi}}{\Gamma(3/4)} (3 - \sqrt{5}) \sqrt{\sqrt{5} - 2} e^{-(\sqrt{5}-2)/2} V_0 \\ & \approx \frac{1}{2} - 1.35V_0. \end{aligned} \quad (28)$$

A detailed analysis of these points will be presented elsewhere.

III. QUADRATIC SOLITONS IN THE FREE SPACE

The stationary solutions of Eq. (5) were constructed by means of the modified squared-operator method [98]. Then,

the stability domains for such stationary states were identified by eigenvalues λ , which were obtained from Eq. (8) with the help of the Fourier collocation method [98]. Finally, the predictions for the stability were verified by direct numerical simulations of the evolution of perturbed solutions in the framework of Eqs. (1) and (2), using the split-step fast-Fourier-transform method. The spatial integration domain we use in this paper is $x \in [-20, 20]$, with a spatial step $dx = 0.05$ and a time step $dt = 0.0005$. The Laplacian-zero boundary condition $(-\partial^2/\partial x^2)^{\alpha/2} \Psi = 0$ (at $x = x_{\min, \max}$) [99, 100] was employed for this work ($x_{\min, \max}$ represent the left and right end point of integration domain, respectively), and we also obtained the same results by using the Neumann boundary condition. Rerunning the simulations in a larger domain, and/or with smaller dx and dt did not produce any conspicuous change in the pictures.

A. Soliton families supported by the spatially uniform quadratic and cubic nonlinearities

Results for solitons produced by Eqs. (1) and (5) in the basic case of the coefficients taken as per Eq. (11) are displayed in Figs. 1 and 2. The soliton families are characterized by the dependence of norm N on chemical potential μ for fixed LI α ,

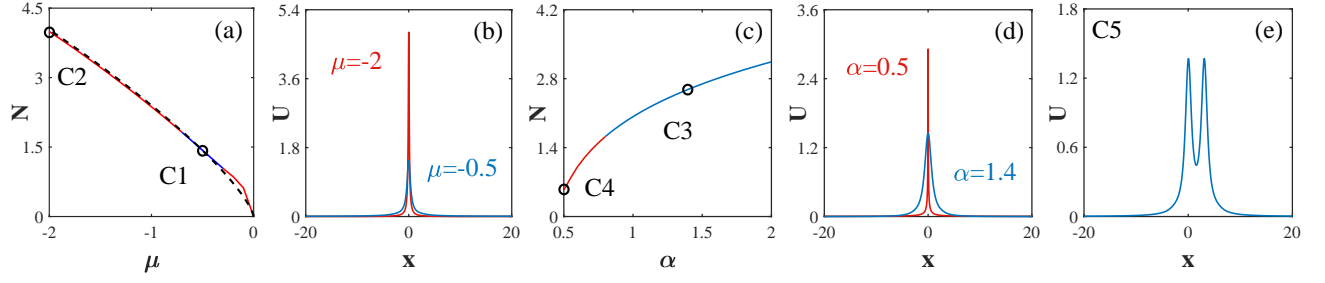


FIG. 5. (a) The dependence $N(\mu)$ and (b) the profiles of solitons labeled C1 and C2 in (a) (corresponding to $\mu = -0.5$ and -2 , respectively) for the soliton family produced by the numerical solution of Eq. (5) with the quadratic nonlinearity subject to the spatially periodic modulations as per Eq. (12), in the absence of the linear potential ($V = 0$), for a fixed LI, $\alpha = 0.8$. (c) The dependence $N(\alpha)$ and (d) the profiles of solitons labeled C3 and C4 (corresponding to $\alpha = 1.4$ and 0.5 , respectively) for a fixed chemical potential, $\mu = -0.6$. The blue and red segments in panels (a) and (c) denote subfamilies of stable and (weakly) unstable solitons, respectively. The black dashed line in (a) represents the analytical scaling relation (10), which corresponds to $\xi(x)$ replaced by its mean value, $\langle \xi(x) \rangle = -0.5$ [see Eq. (12)]. The evolution of the solitons labeled by C1–C4 is displayed in Fig. 6. (e) The shape of the two-peak soliton corresponding to $\alpha = 1.2$ and $\mu = -0.6$. Its perturbed evolution is displayed in Fig. 6(e).

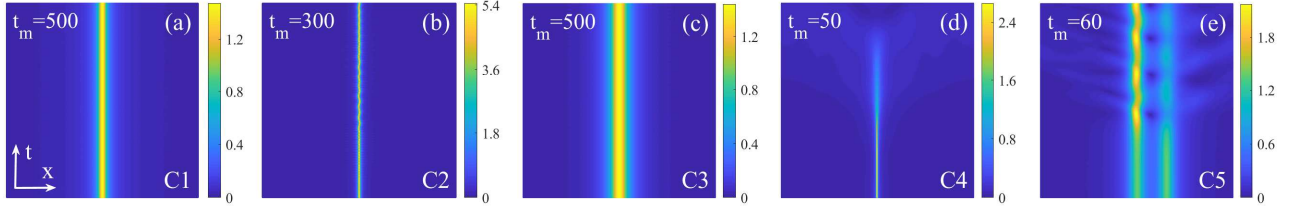


FIG. 6. The perturbed evolution of the solitons corresponding to labels C1–C4 in Figs. 5(a,c). The respective values of the parameters are $\alpha = 0.8$, $\mu = -2$ (a); $\alpha = 0.8$, $\mu = -2$ (b); $\alpha = 1.4$, $\mu = -0.6$ (c); $\alpha = 0.5$, $\mu = -0.6$ (d). Panel (e) displays the perturbed evolution of the double-peak soliton whose stationary shape is presented in Fig. 5(e), for $\alpha = 1.2$, $\mu = -0.6$. Other parameters are given by Eq. (12). In all panels, the evolution is plotted in interval $-10 < x < +10$, while the values t_m indicate time intervals in the respective panels, $0 < t < t_m$.

which is presented in Fig. 1(a) for $\alpha = 0.8$. It is seen that the numerically computed dependence exactly follows the analytical form given by Eq. (12), with properly adjusted constant $N_{\text{quadr}}^{(0)}(\alpha)$. Blue and red segments in the $N(\mu)$ curve identify, respectively, stable and unstable soliton subfamilies. Similar results are produced by the numerical solution for other values of LI from the relevant interval, $0.5 < \alpha \leq 2$.

Further, a typical dependence $N(\alpha)$ for a fixed chemical potential, $\mu = -0.5$, which is also split in stable and unstable segments, is presented in Fig. 1(c). Unlike the $N(\mu)$ dependence, this one cannot be predicted in an exact analytical form. As mentioned above, the VA based on ansatz (17) predicts the approximate value given by Eq. (21) for the degenerate norm of the quasi-Townes solitons, which is relatively close to its numerical counterpart (23). At $\alpha = 2$, the numerical value $N_{\text{numer}}(\alpha = 2) \approx 1.97$ is in complete agreement with the exact analytical value given by Eq. (25).

Typical profiles of the solitons with different values of μ and α , labeled A1–A4 in Figs. 1(a,c), are presented in Figs. 1(b,d) respectively. The fact that the soliton becomes narrower with the increase of $|\mu|$ is another manifestation of the scaling expressed by Eq. (12).

The instability of the solitons belonging to the red segments of the $N(\mu)$ and $N(\alpha)$ dependences in Figs. 1(a,c) is ac-

counted for by a pair of real eigenvalues $\pm\lambda$. For instance, this pair is $\lambda \approx \pm 0.5$ for the weakly unstable soliton shown in Fig. 2(b). The perturbed stable and unstable propagation of the solitons marked A1–A4 in Figs. 1(a,c), whose stationary shapes are shown in Figs. 1(b,d), is displayed in Fig. 2. It is seen that the typical instability is quite weak, giving rise [e.g., in Fig. 2(b)] to small-amplitude intrinsic vibrations of the soliton and emission of virtually invisible linear waves. The instability is very different for the soliton of the Townes type, labeled A4, as seen in Fig. 2(d). It leads to quick decay of the soliton, which is typical for solitons of this type [94].

For comparison with the results summarized in Figs. 1 and 2, systematic findings for solitons supported by the cubic-only nonlinearity in the free space ($V = 0$) are displayed in Figs. 3 and 4 (similar results, but produced by the NLSE with the fractional equation of the Caputo type instead of the Riesz one, were reported in Ref. [101]). In particular, the dependence $N(\mu)$ for such solitons, displayed in Fig. 3(a), completely agrees with the analytically predicted scaling given by Eq. (10). The relationship between N and α for such solitons is presented in Fig. 3(c). As shown in the latter panel, the VA prediction for the norm of the quasi-Townes solitons in the case of the cubic nonlinearity at $\alpha = 1$, given by Eq. (22), is quite close to its numerical counterpart (24). At $\alpha = 2$, the

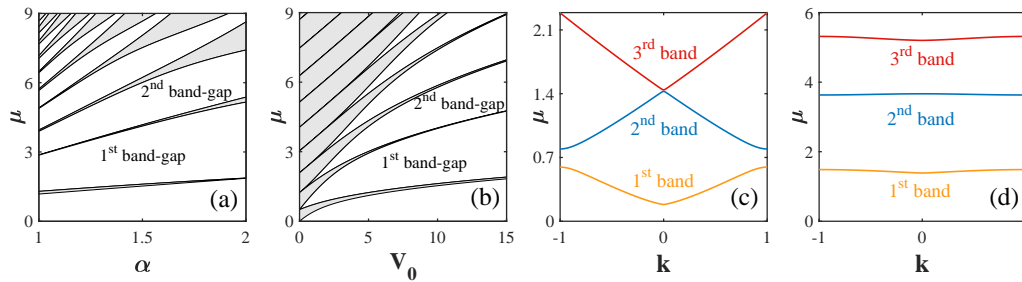


FIG. 7. The bandgap spectrum produced by the linear version of Eq. (1): (a) for different values of the LI α at $V_0 = 8$; (b) for different values of V_0 at $\alpha = 1.3$. The Bloch-wave spectra obtained for different values of V_0 at $\alpha = 1.3$: (c) $V_0 = 0.4$ (a weak lattice potential); (d) $V_0 = 8$ (a strong lattice).

numerically found norm, $N_{\text{numer}}(\alpha = 2) \approx 3.46$, is in complete agreement with the exact analytical value given by Eq. (26).

Profiles of solitons labeled B1–B4 in Figs. 3(a,c) are presented in Figs. 3(b,d), respectively. The perturbed evolution of the stable and unstable solitons is reported, severally, in Figs. 4(a,c) and 4(b,d). It is seen that, in this case too, the instability is relatively weak. It excites intrinsic vibrations of the solitons, without destroying them.

In the case of the mixed QC nonlinearity in the free space, the results are qualitatively similar to those displayed in Figs. 3 and 4. In particular, the mixture of the quadratic and cubic self-attractive terms (with $\xi < 0$ and $g < 0$) makes the stability segments in the $N(\mu)$ and $N(\alpha)$ dependences somewhat broader, although generally similar to those observed in Fig. 3 (not shown here in detail).

B. The quadratic nonlinear lattice

Next we address the system with the quadratic-only nonlinearity, whose local strength is subjected to periodic modulation that represents a nonlinear lattice (while the linear potential is absent). This system is modeled by Eq. (1) with

$$\xi(x) = -\cos^2 x, g = V = 0. \quad (29)$$

where the scaling invariance is used to fix the period of the nonlinear lattice, $L = \pi$, and the center of the soliton may be naturally placed at a local energy minimum, $x = 0$. This setting can be implemented in the LHY liquid by means of the spatially-periodic Feshbach resonance, taking into regard the fact that, in unscaled units, ξ in Eq. (1) is proportional to $|a|^{3/2}$, where a is the scattering length of the atomic collisions in the binary BEC [88] (which, in turn, may be modulated in space by means of a spatially-periodic magnetic field [6]).

Dependences $N(\mu)$ and $N(\alpha)$ for soliton families produced by the numerical solution of stationary equation (5), with parameters taken as per Eq. (29), are displayed in Figs. 5(a,c). It is worthy to note that, although the spatial modulation of $\xi(x)$ breaks the scaling relation (12) between N and μ , the $N(\mu)$ curve in Fig. 5(a) almost exactly obeys this relation, with $\xi(x)$

in Eq. (29) replaced by its mean value, $\langle \xi(x) \rangle = 1/2$. Furthermore, $N(\mu)$ satisfies the VK criterion, even if it is far from being a sufficient stability condition in the present case, since only a relatively small segment of the $N(\mu)$ curve is stable in Fig. 5(a).

Particular examples of fundamental (single-peak) solitons supported by the nonlinear lattice, which are marked by C1–C4 in Figs. 5(a,c), are presented in Figs. 5(b,d), and their perturbed evolution is displayed in Figs. 6(a–d). The shape and dynamical behavior of the solitons are similar to what is shown for their counterparts in the system with $\xi = -1$ in Figs. 1(b,d) and 2. In particular, solution C4, shown in Fig. 5(d), which pertains to $\alpha = 0.5$, represents quasi-Townes solitons in the present case. Accordingly, it suffers fast decay in Fig. 6(d), similar to the instability of its counterpart, shown above in Fig. 2(d).

The nonlinear lattice may support, in addition to the single-peak (fundamental) solitons, also higher-order multi-peak ones. An example of a two-peak soliton is presented in Fig. 5(e), with separation π between the peaks. Both the computation of stability eigenvalues and direct numerical simulations demonstrate that all higher-order solitons supported by the nonlinear lattice are subject to instability, accounted for by a pair of real eigenvalues. In particular, the double-peak soliton shown in Fig. 5(e) is associated with unstable eigenvalues $\lambda \approx \pm 0.3$. Simulations of the perturbed evolution of this soliton, displayed in Fig. 6(e), demonstrate a quick onset of spontaneous symmetry breaking between the two peaks, which is followed by the development of intrinsic vibrations of the stronger peak. This dynamical scenario implies that the attraction between the peaks in the perturbed state is stronger than the effective pinning induced by the nonlinearity modulation in Eq. (29).

IV. GAP SOLITONS (GSS) SUPPORTED BY THE COMPETING QUADRATIC-CUBIC (QC) NONLINEARITY

To address families of GSs supported by the lattice potential (3), it is first necessary to compute the respective bandgap structure, in the framework of the linearization of Eq. (5) (a similar computation was performed in Ref. [59]). The result

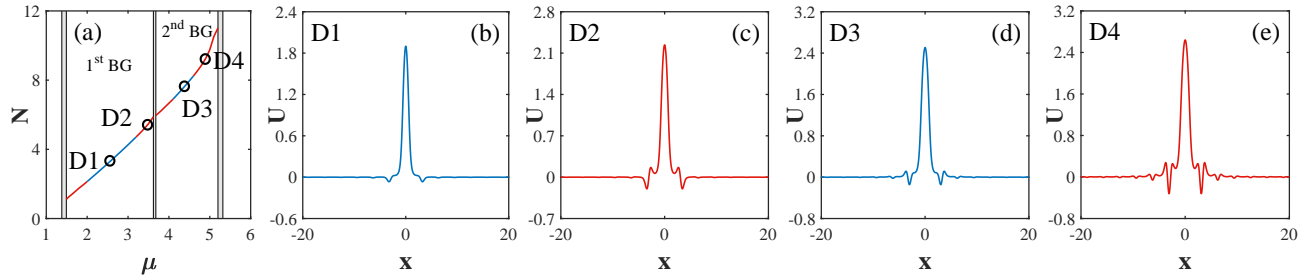


FIG. 8. (a) The norm N of fundamental GSs supported by the competing cubic-quintic nonlinearity, versus their chemical potential μ . The blue and red segments denote stable and unstable GS subfamilies, respectively. The profiles of typical GSs: for $\mu = 2.6$ (b) $\mu = 3.5$ (c); $\mu = 4.4$ (d); and $\mu = 4.9$ (e). The perturbed evolution of the GSs labeled by D1–D4 is displayed in Figs. 11(a1–a4), respectively. For all panels, the parameters in Eq. (1) and (3) are $\alpha = 1.3$, $\xi = -1$, $g = 1$, and $V_0 = 8$.

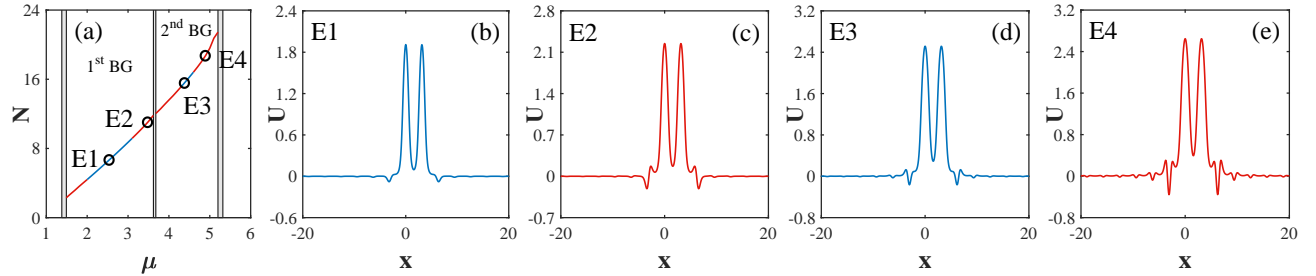


FIG. 9. The same as in Fig. 8, but for two-peak GSs. Their profiles are shown for $\mu = 2.6$ in (b), $\mu = 3.5$ in (c), $\mu = 4.4$ in (d), and $\mu = 4.9$ in (e). The perturbed evolution of the solitons labeled by E1–E4 is displayed in Figs. 11(b1–b4) respectively. In all panels, the parameters are $\alpha = 1.3$, $\xi = -1$, $g = 1$, $V_0 = 8$.

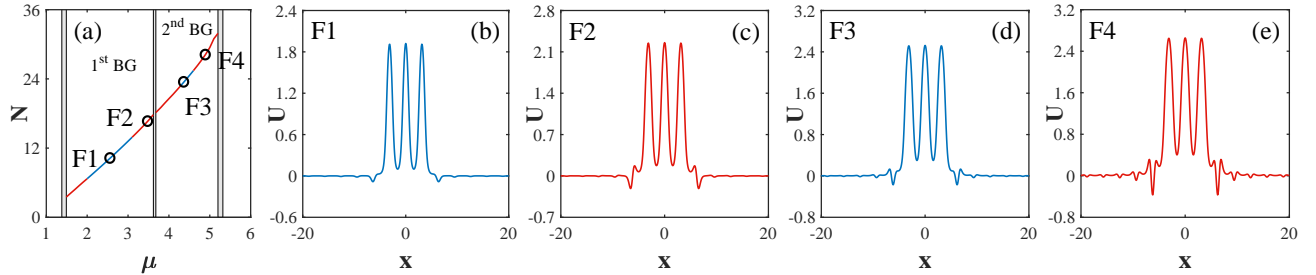


FIG. 10. The same as in Fig. 8, but for three-peak GSs. Their profiles are shown for $\mu = 2.6$ in (b), $\mu = 3.5$ in (c), $\mu = 4.4$ in (d), and $\mu = 4.9$ in (e). The perturbed evolution of the solitons labeled by F1–F4 is displayed in Figs. 11(c1–c4) respectively. In all panels, the parameters are $\alpha = 1.3$, $\xi = -1$, $g = 1$, $V_0 = 8$.

is displayed in Fig. 7. Note that higher-order bandgaps, which may be populated by GSs, appears gradually when the LI α decreases from 2 to 1, or the strength V_0 of the lattice potential increases from 0 to 15, as shown in Figs. 7(a) and (b) respectively. Typical Bloch spectra, in the form of the chemical potential as a function of the quasi-wavenumber, obtained at small and large values of V_0 , are displayed in Figs. 7(c) and (d), respectively. The former plot features a narrow first bandgap and has no second one, while in the latter case both the broad first and second bandgaps are observed in Fig. 7(b).

As mentioned above, GSs produced by the interplay of the self-repulsive or attractive cubic nonlinearity with a lattice po-

tential in the fractal setting were considered in Ref. [59]. It was found that the repulsive sign of the cubic term gives rise to a family of spatially even (symmetric) GSs, which are chiefly stable in the first finite bandgap. GSs of the same type, created by the self-attractive nonlinearity, were completely unstable, but partly stable GSs with an odd (antisymmetric) spatial shape might be supported by the attractive cubic term. Here, we focus on the symmetric GSs, as the most natural species (in particular, it is straightforward to create it in the experiment, by means of a usual laser beam with the Gaussian profile) existing under the combined action of the competing self-attractive quadratic and repulsive cubic terms. Note that the

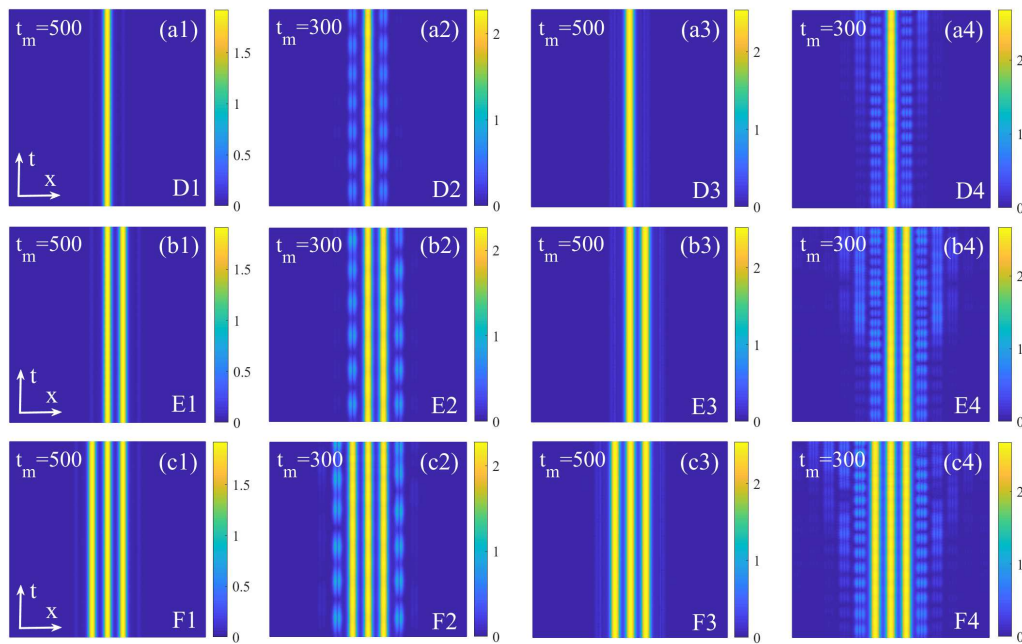


FIG. 11. The perturbed evolution of fundamental, two-, and tree-peak GSs. The panels (a1-a4) correspond to the fundamental solitons labeled D1–D4 in Fig. 8, with values of the chemical potential $\mu = 2.6$ (a1), $\mu = 3.5$ (a2), $\mu = 4.4$ (a3), and $\mu = 4.9$ (a4). The panels (b1-b4) correspond to the two-peak solitons labeled (E1)–(E4) in Fig. 9, with $\mu = 2.6$ (b1), $\mu = 3.5$ (b2), $\mu = 4.4$ (b3), and $\mu = 4.9$ (b4). The panels (c1-c4) correspond to the three-peak solitons labeled (F1)–(F4) in Fig. 10, with $\mu = 2.6$ (c1), $\mu = 3.5$ (c2), $\mu = 4.4$ (c3), and $\mu = 4.9$ (c4). The parameters are $\alpha = 1.3$, $\xi = -1$, $g = 1$, and $V_0 = 8$. In all panels, the evolution is plotted in the interval $-20 < x < +20$, while the values t_m indicate time intervals in the respective panels, $0 < t < t_m$.

setting adopted in Ref. [59] did not allow one to consider competing nonlinearities.

The family of fundamental GSs is displayed in Fig. 8(a) by means of its $N(\mu)$ curve, which covers the first two finite bandgaps, and exhibits alternation of stable (blue) and unstable (red) segments. Note that the curve satisfies the *anti-VK criterion*, $dN/d\mu > 0$, which a necessary stability condition (but, generally speaking, not a sufficient one) for solitons supported by a self-repulsive nonlinearity (in particular, for the usual GSs) [5]. The alternation of actually stable and unstable segments is a nontrivial feature of the present GS family. Qualitatively, it may be construed as a result of the interplay of the trends to stabilize the GSs by the self-repulsive cubic term, and destabilize them by the attractive quadratic one.

The profiles of typical fundamental (single-peaked) GSs in the two lowest bandgaps, labeled by D1–D4 in Fig. 8(a), are plotted in Figs. 8(b–e), respectively, showing that the amplitude of such solitons increases with the growth of μ , and undulations in their shape (represented by additional side extrema) are pronounced stronger near edges of the bandgaps than near their centers. Actually, this feature implies that stable GSs, which are also found closer to the middle of the bandgaps, are smoother than their unstable counterparts.

Numerically simulated perturbed evolution of these fundamental solitons is displayed in Figs. 11(a1–a4), respectively. These numerical simulations suggest that unstable GSs in the first bandgap spontaneously transform into robust breathers,

while in the second bandgap the instability initiates gradual decay of the solitons.

The underlying lattice potential makes it possible to construct multi-peak GSs, which may be considered as bound states of single-peak ones. The resulting family of double-peak GSs is represented in Fig. 9(a) by the respective $N(\mu)$ dependence covering the two lowest bandgaps and showing the alternation of stable (blue) and unstable (red) segments. The comparison of Figs. 9(a) and 8(a) demonstrates that, quite naturally, the power of the two-peak solitons is almost exactly equal to twice the power of their single-peak counterparts.

The profiles of typical two-peak solitons, labeled by E1–E4 in Fig. 9(a), are shown in Figs. 9(b–e), respectively, and their perturbed evolution is displayed in Figs. 11(b1–b4). Similar to their single-peak counterparts shown in Fig. 8, the two-peak GSs develop stronger undulations near the edge of the bandgaps, in comparison to smoother shapes near the bandgaps' centers.

The $N(\mu)$ curve for the family of three-peak GSs, also covering the two lowest bandgaps and separated into stable (blue) and unstable (red) segments, is presented in Fig. 10(a), where it also satisfies the anti-VK criterion. Comparing Figs. 8(a), 9(a) and 10(a), we conclude that the stability intervals are narrower for both the two-peak and three-peak GSs, in comparison to those of the fundamental ones.

Typical profiles of the three-peak solitons, marked by F1–F4 in Fig. 10(a), are plotted in Figs. 10(b–e) respectively,

and their perturbed evolution is displayed in Figs. 11(c1–c4). Similar to what is mentioned above for the two-peak GSs, the power of the three-peak ones is larger almost exactly by a factor of 3 in comparison to the single-peak solitons, and the shape undulations of the three-peak GSs are stronger near the edge of the bandgap. Also similar to the single-peak solitons, those two- and three-peak modes that are unstable, spontaneously transform into oscillating states in the first bandgap, and suffer gradual decay in the second one.

V. CONCLUSION

The objective of this work was to extend the recently developed models of nonlinear fractal waveguides for the case of the quadratic and quadratic-cubic nonlinearities. These models apply to the gas of quantum particles moving by Lévy flights, with the self-attractive nonlinearity representing the LHY correction to the nearly compensated cubic mean-field nonlinearity in the binary BEC. First, the soliton family was constructed in the basic case of the purely quadratic nonlinearity (known as the “LHY liquid”), and the stability of the solitons was investigated. In addition to the numerical findings, some essential results are obtained in the analytical form, such as the $N(\mu)$ dependence, and the value of the degenerate norm of the *quasi-Townes* soliton family, at the value of the Lévy index $\alpha = 1/2$. Solitons supported by the nonlinear lattice, based on the periodically modulated strength of the quadratic term, were briefly considered too, with a conclusion that only the fundamental solitons are stable in this case, all multi-peak ones being unstable.

Next, families of fundamental, double, and triple gap solitons (GSs) were constructed in the first two finite bandgaps, and their stability identified, under the action of the competing quadratic and cubic (attractive and repulsive) terms and

lattice potential. It was found that, due to the presence of the competing nonlinearity, the GS branches split into alternating stable and unstable segments, the solitons tending to be more stable, with a smoother shape, close to the middle of the bandgaps. The stability segments are broader for the fundamental (single-peak) GSs than for the two- and three-peak ones.

This work may be extended in other directions. In particular, it is interesting to construct moving solitons in the free space (note that the fractional diffraction breaks the Galilean invariance of the underlying NLSE, thus making the problem nontrivial), and simulate collisions between them.

FUNDING

National Major Instruments and Equipment Development Project of National Natural Science Foundation of China (61827815); National Natural Science Foundation of China (62075138); Natural Science Foundation of Guangdong Province (2021A1515011909); Science and Technology Project of Shenzhen (JCYJ20190808121817100, JCYJ20190808164007485, JSGG20191231144201722); Natural Science Foundation of Shenzhen University (2019007); Doctoral Scientific Research Foundation of Jiujiang University (8722509); Israel Science Foundation (grant No. 1286/17).

DECLARATION OF COMPETING INTEREST

The authors declare that they have no known competing financial interests or personal relationships that could have appeared to influence the work reported in this paper.

-
- [1] Kivshar YS, Malomed BA. Dynamics of solitons in nearly integrable systems. *Rev Mod Phys* 1989;61(4):763-915.
 - [2] Kivshar YS, Luther-Davies B. Dark optical solitons: physics and applications. *Phys Rep* 1998;298(2-3):81-197.
 - [3] Malomed BA, Mihalache D, Wise F, Torner L. Spatiotemporal optical solitons. *J Opt B* 2005;7(5):R53-R72.
 - [4] Mihalache D. Formation and stability of light bullets: recent theoretical studies. *J Optoelect Adv Mat* 2010;12(1):12-8.
 - [5] Sakaguchi H, Malomed BA. Solitons in combined linear and nonlinear lattice potentials. *Phys Rev A* 2010;81(1):013624.
 - [6] Kartashov YV, Malomed BA, Torner L. Solitons in nonlinear lattices. *Rev Mod Phys* 2011;83(1):247-305.
 - [7] Chen Z, Segev M, Christodoulides DN. Optical spatial solitons: historical overview and recent advances. *Rep Prog Phys* 2012;75(8):086401.
 - [8] Konotop VV, Yang J, Zezyulin DA. Nonlinear waves in \mathcal{PT} -symmetric systems. *Rev Mod Phys* 2016;88(3):035002.
 - [9] Malomed BA. Multidimensional solitons: Well-established results and novel findings. *Eur Phys J Spec Top* 2016;225(13):2507-32.
 - [10] Kartashov YV, Astrakharchik GE, Malomed BA, Torner L. Frontiers in multidimensional self-trapping of nonlinear fields and matter. *Nat Rev Phys* 2019;1(3):185-97.
 - [11] Malomed BA, Mihalache D. Nonlinear waves in optical and matter-wave media: A topical survey of recent theoretical and experimental results. *Rom J Phys* 2019;64:106.
 - [12] Mihalache D. Localized structures in optical and matter-wave media: A selection of recent studies. *Rom Rep Phys* 2021;73(2):403.
 - [13] Pitaevskii LP, Stringari S. *Bose-Einstein Condensation*. Oxford University Press, Oxford, 2003.
 - [14] Bagnato VS, Frantzeskakis DJ, Kevrekidis PG, Malomed BA, Mihalache D. Bose-Einstein condensation: Twenty years after. *Rom Rep Phys* 2015;67:5-50.
 - [15] Borovkova OV, Kartashov YV, Torner L, Malomed BA. Bright solitons from defocusing nonlinearities. *Phys Rev E* 2011;84(3):035602(R).
 - [16] Lobanov VE, Borovkova OV, Kartashov YV, Malomed BA, Torner L. Stable bright and vortex solitons in photonic crystal fibers with inhomogeneous defocusing nonlinearity. *Opt Lett* 2012;37(11):1799-801.

- [17] Driben R, Kartashov YV, Malomed BA, Meier T, Torner L. Three-dimensional hybrid vortex solitons. *New J Phys* 2014;16(6):063035.
- [18] Driben R, Kartashov YV, Malomed BA, Meier T, Torner L. Soliton gyroscopes in media with spatially growing repulsive nonlinearity. *Phys Rev Lett* 2014;112(2):020404.
- [19] Kartashov YV, Malomed BA, Shnir Y, Torner L. Twisted toroidal vortex solitons in inhomogeneous media with repulsive nonlinearity. *Phys Rev Lett* 2014;113(26):264101.
- [20] Kartashov YV, Malomed BA, Vysloukh VA, Belić MR, Torner L. Rotating vortex clusters in media with inhomogeneous defocusing nonlinearity. *Opt Lett* 2017;42(3):446-9.
- [21] Zeng L, Zeng J, Kartashov YV, Malomed BA. Purely Kerr nonlinear model admitting flat-top solitons. *Opt Lett* 2019;44(5):1206-9.
- [22] Zeng L, Zeng J. Gaussian-like and flat-top solitons of atoms with spatially modulated repulsive interactions. *J Opt Soc Am B* 2019;36(8):2278-84.
- [23] Zeng L, Zeng J. Modulated solitons, soliton and vortex clusters in purely nonlinear defocusing media. *Ann Phys* 2020;421:168284.
- [24] Malomed BA, Kevrekidis PG. Discrete vortex solitons. *Phys Rev E* 2001;64(2):026601.
- [25] Baizakov BB, Malomed BA, Salerno M. Multidimensional solitons in periodic potentials. *Europhys Lett* 2003;63(5):642-8.
- [26] Yang J, Musslimani ZH. Fundamental and vortex solitons in a two-dimensional optical lattice. *Opt Lett* 2003;28(21):2094-6.
- [27] Baizakov BB, Malomed BA, Salerno M. Multidimensional solitons in a low-dimensional periodic potential. *Phys Rev A* 2004;70(5):053613.
- [28] Yang J. Stability of vortex solitons in a photorefractive optical lattice. *New J Phys* 2004;6(1):47.
- [29] Brazhnyi VA, Konotop VV. Theory of nonlinear matter waves in optical lattices. *Mod Phys Lett B* 2004;18(14):627-51.
- [30] Mihalache D, Mazilu D, Lederer F, Kartashov YV, Crasovan LC, Torner L. Stable three-dimensional spatiotemporal solitons in a two-dimensional photonic lattice. *Phys Rev E* 2004;70(5):055603.
- [31] Morsch O, Oberthaler M. Dynamics of Bose-Einstein condensates in optical lattices. *Rev Mod Phys* 2006;78(1):179-212.
- [32] Rose P, Richter T, Terhalle B, Imbrock J, Kaiser F, Denz C. Discrete and dipole-mode gap solitons in higher-order nonlinear photonic lattices. *Appl Phys B* 2007;89(4):521-6.
- [33] Zhang Y, Wu B. Composition Relation between Gap Solitons and Bloch Waves in Nonlinear Periodic Systems. *Phys Rev Lett* 2009;102(9):093905.
- [34] Zeng L, Zeng J. Gap-type dark localized modes in a Bose-Einstein condensate with optical lattices. *Adv Photon* 2019;1(4):046004.
- [35] Kartashov YV, Vysloukh VA, Torner L. Propagation of solitons in thermal media with periodic nonlinearity. *Opt Lett* 2008;33(15):1774-6.
- [36] Kartashov YV, Malomed BA, Vysloukh VA, Torner L. Two-dimensional solitons in nonlinear lattices. *Opt Lett* 2009;34(6):770-2.
- [37] Abdullaev FK, Kartashov YV, Konotop VV, Zezyulin DA. Solitons in \mathcal{PT} -symmetric nonlinear lattices. *Phys Rev A* 2011;83(4):041805(R).
- [38] Zeng L, Konotop VV, Lu X, Cai Y, Zhu Q, Li J. Localized modes and dark solitons sustained by nonlinear defects. *Opt Lett* 2021;46(9):2216-9.
- [39] Chen W, Mills DL. Gap solitons and the nonlinear optical response of superlattices. *Phys Rev Lett* 1987;58(2):160-3.
- [40] Eggleton BJ, Slusher RE, de Sterke CM, Krug PA, Sipe JE. Bragg grating solitons. *Phys Rev Lett* 1996;76(10):1627-30.
- [41] Eggleton BJ, de Sterke CM, Slusher RE. Nonlinear pulse propagation in Bragg gratings. *J Opt Soc Am B* 1997;14(11):2980-93.
- [42] Eiermann B, Anker Th, Albiez M, Taglieber M, Treutlein P, Marzlin K-P, Oberthaler MK. Bright Bose-Einstein Gap Solitons of Atoms with Repulsive Interaction. *Phys Rev Lett* 2004;92(23):230401.
- [43] Laskin N. Fractional quantum mechanics and Lévy path integrals. *Phys Lett A* 2000;268(4-6):298-305.
- [44] Laskin N. Fractional quantum mechanics. *Phys Rev E* 2000;62(3):3135-45.
- [45] Laskin N. Fractional Schrödinger equation. *Phys Rev E* 2002;66(5):056108.
- [46] Stickler BA. Potential condensed-matter realization of space-fractional quantum mechanics: The one-dimensional Lévy crystal. *Phys Rev E* 2013;88(1):012120.
- [47] Pinsker F, Bao W, Zhang Y, Ohadi H, Dreismann A, Baumberg JJ. Fractional quantum mechanics in polariton condensates with velocity-dependent mass. *Phys Rev B* 2015;92(19):195310.
- [48] Longhi S. Fractional Schrödinger equation in optics. *Opt Lett* 2015;40(6):1117-20.
- [49] Laskin N. *Fractional quantum mechanics*. World Scientific, Singapore, 2018.
- [50] Zhang Y, Liu X, Belić MR, Zhong W, Zhang Y, Xiao M. Propagation dynamics of a light beam in a fractional Schrödinger equation. *Phys Rev Lett* 2015;115(18):180403.
- [51] Zhang Y, Zhong H, Belić MR, Zhu Y, Zhong W, Zhang Y, Christodoulides DN, Xiao M. \mathcal{PT} symmetry in a fractional Schrödinger equation. *Laser Photonics Rev* 2016;10(3):526-31.
- [52] Secchi S, Squassina M. Soliton dynamics for fractional Schrödinger equations. *Appl Anal* 2014;93(8):1702-29.
- [53] Duo S, Zhang Y. Mass-conservative Fourier spectral methods for solving the fractional nonlinear Schrödinger equation. *Comput Math Appl* 2016;71(11):2257-71.
- [54] Zhong WP, Belić MR, Malomed BA, Zhang Y, Huang T. Spatiotemporal accessible solitons in fractional dimensions. *Phys Rev E* 2016;94(1):012216.
- [55] Zhong WP, Belić MR, Zhang Y. Accessible solitons of fractional dimension. *Ann Phys* 2016;368:110-6.
- [56] Hong Y, Sire Y. A new class of traveling solitons for cubic fractional nonlinear Schrödinger equations. *Nonlinearity* 2017;30(4):1262-86.
- [57] Wang Q, Li J, Zhang L, Xie W. Hermite-Gaussian-like soliton in the nonlocal nonlinear fractional Schrödinger equation. *EPL* 2018;122(6):64001.
- [58] Wang Q, Deng ZZ. Elliptic Solitons in (1+2)-Dimensional Anisotropic Nonlocal Nonlinear Fractional Schrödinger Equation. *IEEE Photonics J* 2019;11(4):1-8.
- [59] Huang C, Dong L. Gap solitons in the nonlinear fractional Schrödinger equation with an optical lattice. *Opt Lett* 2016;41(24):5636-9.
- [60] Xiao J, Tian Z, Huang C, Dong L. Surface gap solitons in a nonlinear fractional Schrödinger equation. *Opt Express* 2018;26(3):2650-8.
- [61] Zhang LF, Zhang X, Wu HZ, Li CX, Pierangeli D, Gao YX, Fan DY. Anomalous interaction of Airy beams in the fractional nonlinear Schrödinger equation. *Opt Express* 2019;27(20):27936-45.
- [62] Dong L, Tian Z. Truncated-Bloch-wave solitons in nonlinear fractional periodic systems. *Ann Phys* 2019;404:57-64.

- [63] Zeng L, Zeng J. One-dimensional gap solitons in quintic and cubic-quintic fractional nonlinear Schrödinger equations with a periodically modulated linear potential. *Nonlinear Dyn* 2019;98(2):985-95.
- [64] Li P, Malomed BA, Mihalache D. Vortex solitons in fractional nonlinear Schrödinger equation with the cubic-quintic nonlinearity. *Chaos Solitons Fract* 2020;137:109783.
- [65] Wang Q, Liang G. Vortex and cluster solitons in non-local nonlinear fractional Schrödinger equation. *J Opt* 2020;22(5):055501.
- [66] Zeng L, Zeng J. One-dimensional solitons in fractional Schrödinger equation with a spatially periodical modulated nonlinearity: nonlinear lattice. *Opt Lett* 2019;44(11):2661-4.
- [67] Qiu Y, Malomed BA, Mihalache D, Zhu X, Peng X, He Y. Stabilization of single- and multi-peak solitons in the fractional nonlinear Schrödinger equation with a trapping potential. *Chaos Solitons Fract* 2020;140:110222.
- [68] Li P, Malomed BA, Mihalache D. Metastable soliton necklaces supported by fractional diffraction and competing nonlinearities. *Opt Express* 2020;28(23):34472-88.
- [69] Zeng L, Mihalache D, Malomed BA, Lu X, Cai Y, Zhu Q, Li J. Families of fundamental and multipole solitons in a cubic-quintic nonlinear lattice in fractional dimension. *Chaos Solitons Fract* 2021;144:110589.
- [70] Zeng L, Zeng J. Preventing critical collapse of higher-order solitons by tailoring unconventional optical diffraction and nonlinearities. *Commun Phys* 2020;3(1):26.
- [71] Molina MI. The fractional discrete nonlinear Schrödinger equation. *Phys Lett A* 2020;384(8):126180.
- [72] Qiu Y, Malomed BA, Mihalache D, Zhu X, Zhang L, He Y. Soliton dynamics in a fractional complex Ginzburg-Landau model. *Chaos Solitons Fract* 2020;131:109471.
- [73] Li P, Li J, Han B, Ma H, Mihalache D. \mathcal{PT} -symmetric optical modes and spontaneous symmetry breaking in the space-fractional Schrödinger equation. *Rom Rep Phys* 2019;71(2):106.
- [74] Li P, Dai C. Double Loops and Pitchfork Symmetry Breaking Bifurcations of Optical Solitons in Nonlinear Fractional Schrödinger Equation with Competing Cubic-Quintic Nonlinearities. *Ann Phys (Berlin)* 2020;532(8):2000048.
- [75] Li P, Malomed BA, Mihalache D. Symmetry breaking of spatial Kerr solitons in fractional dimension. *Chaos Solitons Fract* 2020;132:109602.
- [76] Li P, Li R, Dai C. Existence, symmetry breaking bifurcation and stability of two-dimensional optical solitons supported by fractional diffraction. *Opt Express* 2021;29(3):3193-210.
- [77] Zeng L, Zeng J. Fractional quantum couplers. *Chaos Solitons Fract* 2020;140:110271.
- [78] Zeng L, Shi J, Lu X, Cai Y, Zhu Q, Chen H, Long H, Li J. Stable and oscillating solitons of \mathcal{PT} -symmetric couplers with gain and loss in fractional dimension. *Nonlinear Dyn* 2021;103(2):1831-40.
- [79] Zeng L, Belić MR, Mihalache D, Wang Q, Chen J, Shi J, Cai Y, Lu X, Li J. Solitons in spin-orbit-coupled systems with fractional spatial derivatives. *Chaos Solitons Fract* 2021;152:111406.
- [80] Thirouin J. On the growth of Sobolev norms of solutions of the fractional defocusing NLS equation on the circle. *Ann Inst Henri Poincaré* 2017;AN34(2):509-31.
- [81] Lee TD, Huang K, Yang CN. Eigenvalues and eigenfunctions of a Bose system of hard spheres and its low-temperature properties. *Phys Rev* 1957;106(6):1135-45.
- [82] Petrov DS. Quantum mechanical stabilization of a collapsing Bose-Bose mixture. *Phys Rev Lett* 2015;115(15):155302.
- [83] Hu H, Liu X-J. Microscopic derivation of the extended Gross-Pitaevskii equation for quantum droplets in binary Bose mixtures. *Phys Rev A* 2020;102(4):043302.
- [84] Cabrera C, Tanzi L, Sanz J, Naylor B, Thomas P, Cheiney P, Tarruell L. Quantum liquid droplets in a mixture of Bose-Einstein condensates. *Science* 2018;359(6373):301-4.
- [85] Cheiney P, Cabrera CR, Sanz J, Naylor B, Tanzi L, Tarruell L. Bright soliton to quantum droplet transition in a mixture of Bose-Einstein condensates. *Phys Rev Lett* 2018;120(13):135301.
- [86] Semeghini G, Ferioli G, Masi L, Mazzinghi C, Wolswijk L, Minardi F, Modugno M, Modugno G, Inguscio M, Fattori M. Self-bound quantum droplets of atomic mixtures in free space?. *Phys Rev Lett* 2018;120(13):235301.
- [87] D'Errico A, Burchianti A, Prevedelli M, Salasnich L, Ancilotto F, Modugno M, Minardi F, Fort C. Observation of quantum droplets in a heteronuclear bosonic mixture. *Phys Rev Res* 2019;1(3):033155.
- [88] Petrov DS, Astrakharchik GE. Ultradilute low-dimensional liquids. *Phys Rev Lett* 2016;117(10):100401.
- [89] Astrakharchik GE, Malomed BA. Dynamics of one-dimensional quantum droplets. *Phys Rev A* 2018;98(1):013631.
- [90] Tylutki M, Astrakharchik GE, Malomed BA, Petrov DS. Collective excitations of a one-dimensional quantum droplet. *Phys Rev A* 2020;101(5):051601(R).
- [91] Roati G, Zaccanti M, D'Errico C, Catani J, Modugno M, Simoni A, Inguscio M, Modugno G. ^{39}K Bose-Einstein condensate with tunable interactions. *Phys Rev Lett* 2007;99(1):010403.
- [92] Skov TG, Skou MG, Jørgensen NB, Arlt JJ. Observation of a Lee-Huang-Yang fluid. *Phys Rev Lett* 2021;126(23):230404.
- [93] Vakhitov NG, Kolokolov AA. Stationary solutions of the wave equation in a medium with nonlinearity saturation. *Radiophys Quantum Electron* 1973;16(7):783-9.
- [94] Bergé L. Wave collapse in physics: principles and applications to light and plasma waves. *Phys Rep* 1998;303(5-6):259-370.
- [95] Zeng L, Malomed BA, Mihalache D, Cai Y, Lu X, Zhu Q, Li J. Bubbles and W-shaped solitons in Kerr media with fractional diffraction. *Nonlinear Dyn* 2021;104(4):4253-64.
- [96] Muslih SI, Agrawal OP, Baleanu D. A fractional Schrödinger equation and its solution. *Int J Theor Phys* 2010;49(8):1746-52.
- [97] Desaix M, Anderson D, Lisak M. Variational approach to collapse of optical pulses. *J Opt Soc Am B* 1991;8(10):2082-6.
- [98] Yang J. *Nonlinear Waves in Integrable and Nonintegrable Systems*. SIAM, Philadelphia, 2010.
- [99] Caplan RM, Carretero-González R. Numerical stability of explicit Runge-Kutta finite-difference schemes for the nonlinear Schrödinger equation. *Appl Numer Math* 2013;71:24-40.
- [100] Caplan RM, Carretero-González R. A modulus-squared Dirichlet boundary condition for time-dependent complex partial differential equations and its application to the nonlinear Schrödinger equation. *SIAM J Sci Comput* 2014;36(1):A1-A19.
- [101] Chen M, Zeng S, Lu D, Hu W, Guo Q. Optical solitons, self-focusing, and wave collapse in a space-fractional Schrödinger equation with a Kerr-type nonlinearity. *Phys Rev E* 2018;98(2):022211.